Binary superlattice quantum-well infrared photodetectors for long-wavelength broadband detection

A. R. Ellis and Amlan Majumdar[a)]
Department of Electrical Engineering, Princeton University, Princeton, New Jersey 08544

K. K. Choi
U. S. Army Research Laboratory, Adelphi, Maryland 20783

J. L. Reno
Sandia National Laboratories, Albuquerque, New Mexico 87185

D. C. Tsui
Department of Electrical Engineering, Princeton University, Princeton, New Jersey 08544

We have adopted a binary superlattice structure for long-wavelength broadband detection. In this superlattice, the basis contains two unequal wells, with which more energy states are created for broadband absorption. At the same time, responsivity is more uniform within the detection band because of mixing of wave functions from the two wells. This uniform line shape is particularly suitable for spectroscopy applications. The detector is designed to cover the entire $8–14$ μm long-wavelength atmospheric window. The observed spectral widths are 5.2 and 5.6 μm for two nominally identical wafers. The photoresponse spectra from both wafers are nearly unchanged over a wide range of operating bias and temperature. The background-limited temperature is 50 K at 2 V bias for $F/1.2$ optics. © *2004 American Institute of Physics.* [DOI: 10.1063/1.1764932]

The past decade has seen increased research activity in the area of broadband quantum-well infrared photodetectors (QWIPs) for spectroscopy in the $8–14$ μm atmospheric transmission window.[1–6] Development of on-chip infrared spectrometers requires broadband detector material where wavelength-selective pixels are created using structures such as quantum-grid infrared photodetectors or enhanced QWIPs.[7,8] Initial broadband QWIP designs utilized bound-to-continuum transitions in multiple QW (MQW) and super-lattice (SL) structures.[1,2] These detectors had spectral bandwidths $\Delta\lambda$ of ~ 3 μm (defined as the full-width at half-maxima) and peak wavelengths λ_p in the $5–10$ μm range. Multistack detectors have also been investigated for broadband as well as voltage tunable multicolor detection.[3] Another approach to obtain broadband detection involves MQW structures where each unit consists of several QWs with different well widths and/or well compositions.[4–6] Although these structures have $\Delta\lambda \sim 4.5–6$ μm, large bias voltages are required for obtaining broad response because only the shorter wavelength QWs are turned on at low voltages. Furthermore, since different QWs have different activation energies, their impedance ratio changes with temperature. The resulting change in potential drop leads to different spectral line shapes at different temperatures. In this letter, we present the design and fabrication of long-wavelength broadband QWIPs that employ miniband-to-miniband transitions in binary SL (BSL) structures. These QWIPs have $\Delta\lambda \sim 5–6$ μm with $\lambda_p \sim 10$ μm and exhibit minor changes in bandwidth with bias voltage and temperature.

Superlattice detectors were first introduced by Kastalsky *et al.*[9] Since then, the SL design has been used for both mid-wavelength[10] and long-wavelength[2,11,12] detection. Although these SL detectors have $\Delta\lambda \sim 2–3$ μm, the responsivity spectra are sharply peaked near their cutoff wavelengths.[2,10–12] To further increase the bandwidth and improve the uniformity of the responsivity spectra, we adopted a BSL design. In this structure, the basis of the SL consists of two different wells separated by thin barriers. Upon infrared absorption, electrons from each of the two ground minibands that originate from the two QWs are photoexcited to the two upper minibands, thus greatly expanding the spectral coverage. The mixing of states among the unequal wells also changes the energy distribution of oscillator strength. By adjusting the BSL parameters, different degrees of mixing can be obtained, which results in different line shapes. Therefore, the BSL design greatly increases detector versatility for broadband applications.

In the present BSL design for the $8–14$ μm range, we found that only a slight difference in the well widths is needed, for which the respective minibands are merged together. Nevertheless, the BSL design is useful because the strong mixing of the nearly degenerate states enables a uniform spectral responsivity within the detection band. The detector contains an active region sandwiched between 0.1 μm (top) and 1 μm (bottom) doped GaAs contact layers. The active region consists of 18 periods of alternating uniformly doped BSLs ($N_d = 4 \times 10^{17}$ cm^{-3} Si) with 600 Å Al$_{0.19}$Ga$_{0.81}$As blocking barriers. The BSL, illustrated in Fig. 1, contains four units of a two well basis made from one 70 Å and one 75 Å GaAs well. The wells are separated from each other and from the blocking barriers by 25 Å Al$_{0.27}$Ga$_{0.73}$As barriers. The entire structure is grown on semi-insulating (100)-GaAs by molecular beam epitaxy. Two nominally identical structures were grown—one at Sandia National Laboratories and another at IQE.[13]

[a)]Author to whom correspondence should be addressed; present address: Components Research, Intel Corporation, 5200 NE Elam Young Parkway, Hillsboro, OR 97124; electronic mail: amlan.majumdar@intel.com

Report Documentation Page

1. REPORT DATE **21 JUN 2004**	2. REPORT TYPE	3. DATES COVERED **-**

4. TITLE AND SUBTITLE **Binary superlattice quantum-well infrared photodetectors for long-wavelength broadband detection**	5a. CONTRACT NUMBER **F29601-02-C-0267**
	5b. GRANT NUMBER
	5c. PROGRAM ELEMENT NUMBER **62601F**

6. AUTHOR(S) **A Ellis; Amlan Majumdar; K Choi; J Reno; D Tsui**	5d. PROJECT NUMBER **4846**
	5e. TASK NUMBER **CR**
	5f. WORK UNIT NUMBER **A1**

7. PERFORMING ORGANIZATION NAME(S) AND ADDRESS(ES) **Department of Electrical Engineering,Princeton University,Princeton,NJ,08544**	8. PERFORMING ORGANIZATION REPORT NUMBER

9. SPONSORING/MONITORING AGENCY NAME(S) AND ADDRESS(ES)	10. SPONSOR/MONITOR'S ACRONYM(S)
	11. SPONSOR/MONITOR'S REPORT NUMBER(S)

12. DISTRIBUTION/AVAILABILITY STATEMENT **Approved for public release; distribution unlimited**

13. SUPPLEMENTARY NOTES

14. ABSTRACT
We have adopted a binary superlattice structure for long-wavelength broadband detection. In this superlattice, the basis contains two unequal wells, with which more energy states are created for broadband absorption. At the same time, responsivity is more uniform within the detection band because of mixing of wave functions from the two wells. This uniform line shape is particularly suitable for spectroscopy applications. The detector is designed to cover the entire 8-14 μm long-wavelength atmospheric window. The observed spectral widths are 5.2 and 5.6 μm for two nominally identical wafers. The photoresponse spectra from both wafers are nearly unchanged over a wide range of operating bias and temperature. The background-limited temperature is 50 K at 2 V bias for F/1.2 optics.

15. SUBJECT TERMS

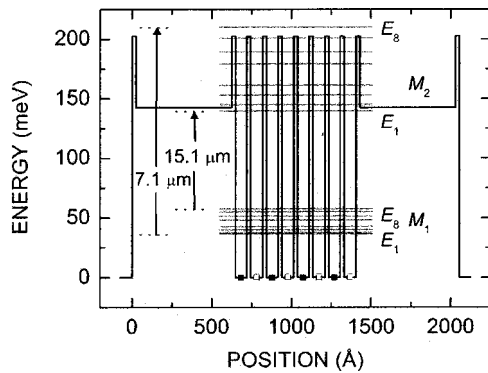| 16. SECURITY CLASSIFICATION OF:			17. LIMITATION OF ABSTRACT	18. NUMBER OF PAGES **4**	19a. NAME OF RESPONSIBLE PERSON
a. REPORT **unclassified**	b. ABSTRACT **unclassified**	c. THIS PAGE **unclassified**			

FIG. 1. Conduction band profile (black) and calculated energy levels (grey) of one period of the binary SL structure. Alternate GaAs QWs are 70 Å (closed squares) and 75 Å (open squares) wide. The first and second minibands, M_1, and M_2, both contain eight energy levels with E_1 being the lowest and E_8 the highest. The arrows indicate transitions that correspond to the shortest and the longest possible peak detection wavelengths.

We calculated the energy levels and wave functions of one period of the BSL structure using the transfer matrix method.[10,14,15] As shown in Fig. 1, the BSL has two minibands $(M_1$ and $M_2)$ containing eight energy levels each $(E_1 - E_8)$. We found that the lack of translational symmetry in the finite BSL breaks the selection rule for optical transitions, allowing more optical transitions than in SLs with identical wells. The shortest and the longest possible peak detection wavelengths are 7.1 μm $(M_1E_1 \rightarrow M_2E_8)$ and 15.1 μm $(M_1E_8 \rightarrow M_2E_1)$, respectively. Since these wavelengths depend on the BSL miniband structure, they can be tailored by varying the BSL parameters. In addition, the cutoff wavelength can also be controlled by the doping density N_d if all states in M_1 are not occupied. In this case, as N_d is increased, the higher subbands in M_1 are progressively occupied, allowing longer wavelength transitions.

We further elaborate the above-mentioned issue by plotting the calculated absorption spectra in Fig. 2 for $N_d = 3$ and 4×10^{17} cm^{-3}. These spectra were calculated from the computed values of oscillator strength and electron population in energy levels E_1 through E_8 in M_1 at $T = 0$ K. We further assumed that all transitions have a Gaussian line shape due to inhomogeneous broadening.[10] The width of the Gaussian distribution is $\sigma_E = 11$ and 0.5 meV for the solid and the dashed curves in Fig. 2, respectively. The value of $\sigma_E = 11$ meV is expected for monolayer fluctuations in well and
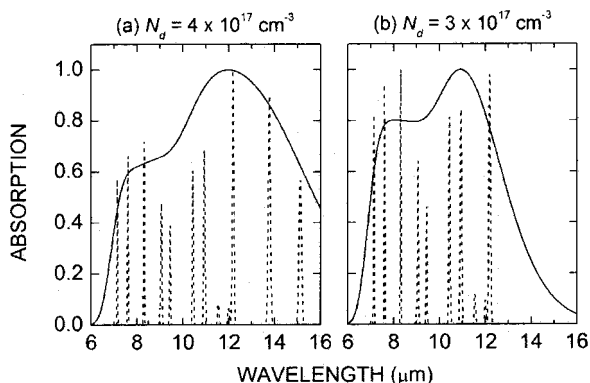

FIG. 2. Calculated absorption spectra of the binary SL QWIP for doping densities N_d of (a) 4×10^{17} cm^{-3} and (b) 3×10^{17} cm^{-3}. Individual transitions are assumed to have Gaussian broadening with width $\sigma_E = 11$ meV (solid lines) and 0.5 meV (dashed lines).
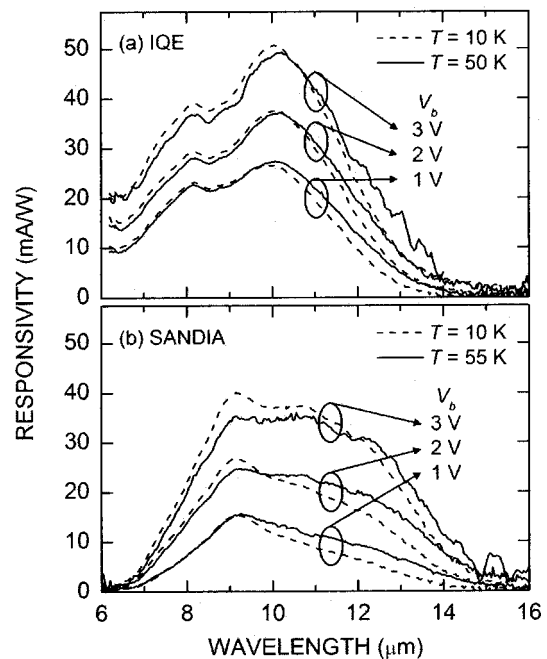

FIG. 3. Spectral responsivity of edge-coupled detectors processed from binary SL wafers grown at (a) IQE and (b) Sandia. The applied bias $V_b = 3$, 2, and 1 V (top to bottom curve) while the detector temperature $T = 10$ K (dashed lines) and 50 K (solid lines).

barrier widths,[2] while the smaller value of $\sigma_E = 0.5$ meV reveals the contribution of the individual transitions. At the nominal doping density of $N_d = 4 \times 10^{17}$ cm^{-3} [Fig. 2(a)], all eight subbands in M_1 are occupied, which leads to a broad absorption spectrum with $\Delta\lambda = 8.6$ μm and cutoff wavelength $\lambda_c = 15.8$ μm. For the lower doping density of $N_d = 3 \times 10^{17}$ cm^{-3} [Fig. 2(b)], only subbands $E_1 - E_6$ in M_1 are occupied. Since less energy levels in M_1 take part in optical transitions, the absorption spectrum is narrower with $\Delta\lambda = 6$ μm and $\lambda_c = 13$ μm. This example shows that a small change in the Fermi level (~ 4 meV at low temperatures) can lead to a substantial reduction of λ_c (~ 3 μm change). Therefore, a partially filled M_1 is not an optimum design because λ_c is reduced while the activation energy for dark current is virtually unchanged. Figure 2 indicates smooth absorption spectra for both doping levels, which is due to the large number of allowed transitions in the BSL.

We processed 45° edge-coupled devices to characterize our detectors. The responsivity spectra of a typical device from both the IQE and Sandia wafers are shown in Fig. 3 as a function of positive voltage bias V_b (referenced to the bottom contact) and temperature T. The negative bias spectra are narrower than the positive bias ones, and hence, are not presented here. The IQE detector spectra are only slightly affected by V_b and T with $\leqslant 5\%$ change in λ_p and $\Delta\lambda$. The widest spectrum is obtained at $V_b = 3$ V and $T = 50$ K and has $\lambda_p = 10$ μm, $\Delta\lambda = 5.2$ μm$(\Delta\lambda/\lambda_p = 52\%)$, and cut-on and cut-off wavelengths of 7 and 12.2 μm, respectively. The Sandia device spectra are shifted toward longer wavelengths compared to those of the IQE device. The widest spectrum for this detector occurs at $V_b = 3$ V and $T = 55$ K, where $\lambda_p = 9.2$ μm and $\Delta\lambda = 5.6$ μm$(\Delta\lambda/\lambda_p = 61\%)$. The cut-on and cutoff wavelengths are 7.9 and 13.5 μm, respectively, which shows that this detector is able to cover the entire 8–14 μm atmospheric window. For a fixed T, we observe an enhancement of the long-wavelength response and $\sim 20\%$ increase in

Appl. Phys. Lett., Vol. 84, No. 25, 21 June 2004

Ellis *et al.* 5129

$\Delta\lambda$ with increasing bias in the 1–3 V range. Also, at a fixed $V_b, \Delta\lambda$ increases by ~10% as T is raised from 10 to 55 K, which can be attributed to thermal broadening of M_1 by ~4 meV.

The discrepancies between the two wafers can be attributed to different QW widths and doping densities. If the QWs are a little narrower than their nominal widths, all energy levels increase slightly; however, the effect is larger for M_2. Consequently, all detection peaks are blueshifted. This increase in energy not only pushes out the level M_2E_1 into the quasicontinuum above the blocking barrier [see Fig. 1] but also enhances the escape probability of photoexcited electrons from M_2. These effects would lead to negligible bias dependence of the spectral width as observed for the IQE detector. Therefore, the QWs in the IQE wafer are probably narrower than the designed ones. On the other hand, if the QWs are slightly wider than the nominal ones, the subband energies would decrease slightly, which would lead to a reduction of the escape probability of low-energy photoelectrons from states such as M_2E_1. However, the tunneling probability of the low-energy photocarriers through the tip of the wide blocking barriers increases with bias voltage. Since the low-energy subbands in M_2 are the final states for the long-wavelength optical transitions, we expect wider responsivity spectra at higher bias. This trend is consistent with the bias dependence of spectral width of the Sandia wafer. Therefore, we conclude that the QW widths in the Sandia wafer are a little larger than their nominal value. We confirmed this with x-ray diffraction analysis, which indicates that the actual period of the BSL structure is 1477 Å, which is about 5% larger than the nominal value of 1405 Å.

The widest bandwidths obtained for both wafers are comparable to the best ones achieved by other groups so far.[4–6] For the IQE device, the responsivity line shape and bandwidth are very similar to those of the calculated absorption spectra for the lower N_d of 3×10^{17} cm^{-3}. The IQE sample is, therefore, consistent with a structure that has a lower N_d and an energy independent escape probability as discussed earlier. On the other hand, the Sandia detector gives a broader spectrum, which indicates that the doping level is closer to the nominal value. However, λ_c in this case is limited by the tunneling probability of photoelectrons below the blocking barrier, which shortens λ_c to 13.5 μm at $V_b=3$ V. Nevertheless, the reduced escape probability toward longer wavelengths produces more uniform responsivity spectra, which are suitable for spectroscopy applications.

Dark current density J_d of both detectors is plotted in Fig. 4 for the 30–70 K temperature range. We have also plotted the window photocurrent density J_w that was generated by 300 K background radiation incident through $F/1.2$ optics. The detector temperature was fixed at 10 K for this measurement. Figure 4 shows that both detectors have a background-limited temperature $T_{\rm BLIP}$, defined as the temperature where $J_d=J_w$, of 55, 50, and 40 K at $V_b=1, 2$, and 3 V, respectively. These values of $T_{\rm BLIP}$ are comparable to those of QWIPs with similar cutoff wavelengths but narrower bandwidths.[14] We also prepared corrugated-QWIPs (C-QWIPs) from both wafers for normal-incidence detection.[16] The responsivity spectra of the C-QWIPs are similar to those of the 45° edge-coupled devices.
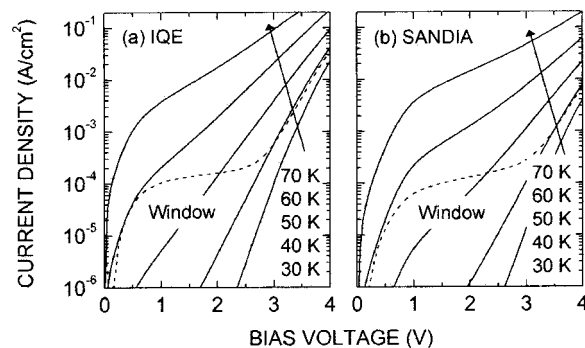

FIG. 4. Bias V_b dependence of dark current density J_d (solid lines) and window photocurrent density J_w (dashed lines) of binary SL detectors grown at (a) IQE and (b) Sandia. The detector temperature $T=70, 60, 50, 40$, and 30 K (top to bottom curve) for the J_d–V_b curves while $T=10$ K for the J_w–V_b curve.

In conclusion, a long-wavelength broadband QWIP using a SL with a binary basis was demonstrated. This BSL structure offers greater flexibility in spectral coverage and line shape. In addition, there is little dependence of the detector spectra on bias and temperature. The background-limited temperature is similar to those of standard QWIPs with similar cutoff wavelengths. The BSL is adequate for the 8–14 μm atmospheric window. For even wider bandwidths, one can further increase the number of QWs in the basis.

[1] B. F. Levine, G. Hasnain, C. G. Bethea, and N. Chand, Appl. Phys. Lett. **54**, 2704 (1989).
[2] S. D. Gunapala, B. F. Levine, and N. Chand, J. Appl. Phys. **70**, 305 (1991).
[3] H. C. Liu, J. Li, J. R. Thompson, Z. R. Wasilewski, M. Buchanan, and J. G. Simmons, IEEE Electron Device Lett. **14**, 566 (1993).
[4] S. V. Bandara, S. D. Gunapala, J. K. Liu, E. M. Luong, J. M. Mumolo, W. Hong, D. K. Sengupta, and M. J. McKelvey, Appl. Phys. Lett. **72**, 2427 (1998).
[5] J. Chu, S. S. Li, and A. Singh, IEEE J. Quantum Electron. **35**, 312 (1999).
[6] J. H. Lee, S. S. Li, M. Z. Tidrow, W. K. Liu, and K. Bacher, Appl. Phys. Lett. **75**, 3207 (1999).
[7] K. K. Choi, C. H. Lin, K. M. Leung, and T. Tamir, Proc. SPIE **4795**, 27 (2002).
[8] P. Mitra, F. C. Case, J. H. McCurdy, S. A. Zaidel, and L. T. Claiborne, Appl. Phys. Lett. **82**, 3185 (2003).
[9] A. Kastalsky, T. Duffield, S. J. Allen, and J. Harbison, Appl. Phys. Lett. **52**, 1320 (1988).
[10] K. K. Choi, S. V. Bandara, S. D. Gunapala, W. K. Liu, and J. M. Fastenau, J. Appl. Phys. **91**, 551 (2002).
[11] K. M. S. V. Bandara, J. W. Choe, M. H. Francombe, A. G. U. Perera, and Y. F. Lin, Appl. Phys. Lett. **60**, 3022 (1992).
[12] C. C. Chen, H. C. Chen, C. H. Kuan, S. D. Lin, and C. P. Lee, Appl. Phys. Lett. **80**, 2251 (2002).
[13] IQE Inc., 119 Technology Drive, Bethlehem, PA 18015.
[14] K. K. Choi, *The Physics of Quantum Well Infrared Photodetectors* (World Scientific, River Edge, NJ, 1997).
[15] In our calculations, we assumed that the BSL is under flatband condition, which is valid even when the entire structure is under an applied bias because the resistance of the BSL is much smaller than that of the adjacent blocking barriers.
[16] C. J. Chen, K. K. Choi, M. Z. Tidrow, and D. C. Tsui, Appl. Phys. Lett. **68**, 1446 (1996).